Organic Electronics 120 (2023) 106846

Contents lists available at ScienceDirect

Organic Electronics

journal homepage: www.elsevier.com/locate/orgel

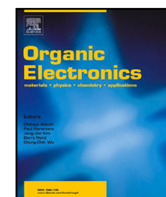

Compact model for the bias-depended low-frequency noise in organic thin-film transistors due to carrier-number and mobility-fluctuation effects ☆

Aristeidis Nikolaou [b,*], Jakob Leise [a,b], Ute Zschieschang [d], Hagen Klauk [d], Thomas Gneiting [c], Ghader Darbandy [a], Benjamin Iñiguez [b], Alexander Kloes [a]

[a] NanoP, TH Mittelhessen University of Applied Sciences, 35390 Giessen, Germany
[b] DEEEA, Universitat Rovira i Virgili, Tarragona, Spain
[c] AdMOS GmbH, Frickenhausen, 72636, Germany
[d] Max Planck Institute for Solid State Research, Stuttgart 70569, Germany

ARTICLE INFO

Keywords:
Low-frequency noise
Carrier-number fluctuation
Mobility fluctuation
Organic thin-film transistors

ABSTRACT

A charge-based compact model for the bias-dependent low-frequency noise in organic thin-film transistors is presented. The model combines the carrier-number fluctuation effect and the fluctuation of the carrier mobility according to the Hooge model to predict the drain-current noise. The model has been verified using experimental data from a large number of organic transistors with two different channel lengths fabricated in the inverted staggered device architecture on a flexible polymeric substrate.

1. Introduction

In organic thin-film transistors (TFTs), the semiconductor is a thin, usually polycrystalline layer of conjugated organic molecules [1]. Organic TFTs are typically fabricated at relatively low process temperatures, i.e., below about 100 °C [2], and can thus be utilized as building blocks in flexible electronics applications [3]. The efficient design of electronic systems is accomplished with the help of circuit simulators, which require physics-based compact models that accurately predict the electrical behavior of the transistors. Physics-based compact models need to cover a wide range of transistor properties, such as DC behavior [4,5], AC behavior [6], short-channel effects [7], drain-current variability [8,9] and low-frequency noise (LFN). In organic TFTs, LFN is dominated mainly by carrier-number fluctuations due to grain-boundary traps, and less by carrier scattering at the semiconductor–dielectric interface [10]. Accurate LFN modeling of organic TFTs has been successfully demonstrated by adopting the theory of carrier-number-correlated mobility fluctuations [11,12] and the empirical Hooge approach [13–15].

In this study, a bias-dependent model for the drain-current low-frequency noise (LFN) in organic TFTs is introduced. The charged-based model proposed here takes into account the two discrete effects that constitute the sources of the flicker noise in organic TFTs, namely the noise due to the carrier-number and correlated mobility-fluctuation effect (ΔN or McWorther model [16]) and the noise due to the fluctuation of the charge-carrier mobility ($\Delta\mu$ or Hooge model [17]). As a result, the model is more flexible in accurately predicting the bias-dependent behavior of LFN in organic TFTs of the inverted staggered device architecture, from the subthreshold regime to the maximum-effective-gate-voltage regime. Additionally, the LFN-model equations are fully combined with a current–voltage compact model for organic TFTs [4, 18], and the complete model is implemented in Verilog-A [19]. For the verification, a large number of organic transistors were fabricated and characterized.

2. LFN model derivation

In this section, the derivation of a drain-current LFN model suitable for organic TFTs is presented. As mentioned above, the proposed model treats the flicker noise as the sum of two contributions, namely the noise due to ΔN effects and the noise due to $\Delta\mu$ effects.

For the LFN noise model derived here, the charge-based organic-TFT current–voltage model described in [4] will be used as the basis. The proposed model provides a single current equation that is valid for all operation regions and can be obtained from

$$I_{DS} = \mu W \left(U_T \frac{Q_S - Q_D}{L} + \frac{Q_S^2 - Q_D^2}{2LC'_{ox}} \right), \tag{1}$$

☆ This project is funded by the German Federal Ministry of Education and Research ("SOMOFLEX", No. 13FH015IX6) and the German Research Foundation (DFG) under the grant KL 1042/9-2 (SPP FFlexCom).

* Corresponding author at: DEEEA, Universitat Rovira i Virgili, Tarragona, Spain.
E-mail addresses: aristeidis.nikolaou@estudiants.urv.cat (A. Nikolaou), alexander.kloes@ei.thm.de (A. Kloes).

https://doi.org/10.1016/j.orgel.2023.106846
Received 19 February 2023; Received in revised form 11 May 2023; Accepted 11 May 2023
Available online 16 May 2023
1566-1199/© 2023 Elsevier B.V. All rights reserved.

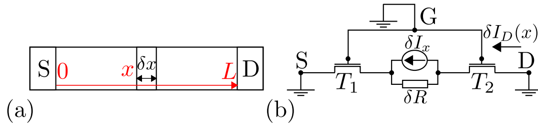

Fig. 1. (a) Schematic of a transistor channel divided into a noisy element located between the positions x and $x + \delta x$ and two noiseless pseudo-transistors having channel lengths x and $L - x$, respectively. (b) Small-signal representation [8].

where $U_T = kT/q$ is the thermodynamic voltage, W is the channel width, L is the channel length, C'_{ox} is the unit-area gate-dielectric capacitance, and μ is the effective carrier mobility. Q_S and Q_D are the densities of quasi-mobile charges per gate area at the source and drain ends of the channel, respectively, and can be expressed as

$$Q_{S(D)} = aU_T C'_{ox} \mathcal{L} \left\{ \exp\left(\frac{V_{GS(D)} - V_{T0}}{aU_T} \right) \right\}, \tag{2}$$

where $\mathcal{L}$ is the first branch of the Lambert W function, a is the sub-threshold slope factor and V_{T0} is the threshold voltage. The DC model was also extended to cover short-channel and contact resistance effects on the drain-current characteristics [7,20].

2.1. ΔN Model derivation

Here, the impact of local charge-density fluctuations in the carrier channel as one of the sources of the drain-current LFN in organic TFTs will be discussed. This noise originates from local random fluctuations of the carrier density or carrier velocity, leading to a local fluctuation of the drain current [14]. The fluctuation of the drain current around its nominal value is thus considered to be a result of the sum of all local fluctuation contributions along the channel. Following the methodology described in [21] for silicon transistors and in [8] for organic TFTs, the transistor channel is divided into a noisy element located between the positions x and $x + \delta x$ and two noiseless pseudo-transistors T1 and T2 that have channel lengths x and $L-x$, respectively (see Fig. 1). The relative local current fluctuation at the position x of the channel can be described as [8]

$$\frac{\delta I_x}{I_D} = \frac{\delta I_D(x)}{I_D} = \frac{\delta Q_{CH}}{Q_{CH}} + \frac{\delta\beta}{\beta}, \tag{3}$$

where the term $\delta\beta/\beta$ describes the charge-trapping effects or edge effects [22] on $\beta = \mu C'_{ox}\frac{W}{L}$. Attributing all variations exclusively to charge trapping, and by following [23], based on Matthiessen's rule, the carrier mobility, including the effect of the trapping mechanism, can be expressed as

$$\frac{1}{\mu} = \frac{1}{\mu_0} + a_c Q_t \Leftrightarrow \mu = \frac{\mu_0}{1 + a_c Q_t \mu_0}, \tag{4}$$

where $Q_t = -qN_t$ is the density of trapped charges and $a_c = \tilde{a_c}/q$ is the Coulomb scattering coefficient [21]. Using (4), the following can be obtained:

$$\frac{\delta\beta}{\delta Q_t} = -\, a_c \mu \beta \tag{5}$$

and the relative current fluctuation can be expressed as

$$\frac{\delta I_D(x)}{I_D} = \left(\frac{1}{Q_{CH}} \frac{\delta Q_{CH}}{\delta Q_t} - a_c \mu \right) \delta Q_t, \tag{6}$$

where δQ_t is the local charge fluctuation related to the fluctuation in the trap density. Furthermore, according to [8], the following can be obtained

$$\frac{\delta Q_{CH}}{\delta Q_t} \simeq \frac{Q_{CH}}{Q_{CH} + Q^*/a} = \frac{q_{ch}}{q_{ch} + 1/a}. \tag{7}$$

Similar to some of the widely-used commercial compact models (i.e. BSIM-BULK, EKV) [21,24], charges are normalized according to

$$\frac{Q_{CH}}{q_{ch}} = \frac{Q_D}{q_d} = \frac{Q_S}{q_s} = Q^*, \tag{8}$$

where

$$Q^* = aU_T C'_{ox}. \tag{9}$$

The terms q_s and q_d are the normalized charge densities at the source and drain ends of the channel, respectively. By substituting (7) into (6), the relative local current fluctuation can be rewritten as

$$\frac{\delta I_D(x)}{I_D} = \left(\frac{1}{q_{ch} + 1/a} + a^* \mu \right) \frac{\delta Q_t}{Q^*}, \tag{10}$$

where $a^* = a_c(-Q^*)$ is a parameter related to the Coulomb scattering coefficient given in units of Vs/m^2. Accordingly, the power spectral density (PSD) of the local noise current source δI_x, normalized to the square of the drain current, is expressed as [21]

$$\frac{S_{\delta I_x^2}}{I_D^2} = \left(\frac{1}{q_{ch} + 1/a} + a^* \mu \right)^2 \frac{S_{\delta Q_t^2}}{(Q^*)^2}. \tag{11}$$

The PSD $S_{\delta Q_t^2}$ is given by

$$S_{\delta Q_t^2} = \frac{kTq^2 \lambda N_T}{W \delta x f^{AF}}, \tag{12}$$

where f is the frequency, AF is the frequency-exponent [25], k is the Boltzmann constant, T is the temperature, λ is the tunneling attenuation distance and N_T is the gate-dielectric volumetric trap density per unit energy (in units of eV^{-1} m^{-3}).

Following [21], by integrating along the transistor channel, the PSD of the total drain-current fluctuation S_{I_D}, normalized to the square of the total drain current, can be expressed as

$$\left.\frac{S_{ID}}{I_D^2}\right|_{\Delta N} = \frac{1}{L^2} \int_0^L \delta x \frac{S_{\delta I_x^2}}{I_D^2} dx, \tag{13}$$

and by substituting Eqs. (9), (11) and (12) into (13), the following can be obtained:

$$\left.\frac{S_{ID}}{I_D^2}\right|_{\Delta N} = \frac{q^4 \lambda N_T}{W L^2 a^2 kT C'^2_{ox} f^{AF}} \int_0^L \left(\frac{1}{q_{ch} + 1/a} + a^* \mu \right)^2 dx. \tag{14}$$

Solving the integral above yields:

$$\left.\frac{S_{ID}}{I_D^2}\right|_{\Delta N} = C^*_{noise}|_{\Delta N} \times B^*_{noise}(q_{ch})|_{\Delta N} \tag{15}$$

where

$$C^*_{noise}|_{\Delta N} = \frac{q^4 \lambda N_T}{W L a^2 kT C'^2_{ox} f^{AF}} \tag{16}$$

and

$$B^*_{noise}(q_s, q_d)|_{\Delta N} = \frac{1}{i_d} \left(B_1 + B_2 + B_3 + B_4 \right). \tag{17}$$

The coefficients B_1, B_2, B_3 and B_4 are given by

$$\begin{aligned} B_1 &= \left(\frac{2(a-1)a^*\mu}{a} + 1 \right) ln \left(\frac{1 + aq_s}{1 + aq_d} \right), \\ B_2 &= \left(\frac{1-a}{1 + aq_s} - \frac{1-a}{1 + aq_d} \right), \\ B_3 &= i_d \left(a^* \mu \right)^2, \\ B_4 &= 2 \left(a^* \mu \right) \left(q_s - q_d \right). \end{aligned} \tag{18}$$

The normalized drain current i_d can be expressed as $i_d = I_D/\mu(aU_T)^2 C'_{ox}W/L$. Similarly as demonstrated previously for silicon transistors [26,27], the results we obtained for the $1/f$ noise in organic TFTs are closely related to those derived in [8] for the drain-current variability, since the physical mechanisms at the origin of both phenomena are similar.

2.2. Δμ Model derivation

The drain-current flicker noise arising from the fluctuations of the carrier mobility can be modeled using the so-called Hooge (Δμ) model.

Accordingly, the total PSD of a local noise-current source δI_x due to the delta μ effect can be expressed as [21]

$$\left.\frac{S_{\delta I_x^2}}{I_D^2}\right|_{\Delta\mu} = \frac{a_H q}{W\delta x(-Q_{ch})f^{AF}}, \tag{19}$$

where a_H is the unitless Hooge parameter. By using Eq. (13) and integrating along the channel, the PSD of the total fluctuation of the drain current due to the $\Delta\mu$ effect, normalized to the square of the total drain current, is then given by

$$\left.\frac{S_{ID}}{I_D^2}\right|_{\Delta\mu} = C^*_{noise}|_{\Delta\mu} \times B^*_{noise}(q_{ch})|_{\Delta\mu}, \tag{20}$$

where

$$C^*_{noise}|_{\Delta\mu} = \frac{a_H q^2}{WLkTaC'_{ox}f^{AF}} \tag{21}$$

and

$$B^*_{noise}|_{\Delta\mu} = \frac{1}{i_d}(lnq_s - lnq_d + q_s - q_d) \tag{22}$$

is the bias-dependent factor.

2.3. Total drain-current low-frequency noise

The total LFN as the sum of the two noise sources described above can be expressed as follows:

$$\frac{S_{ID}}{I_D^2} = \left.\frac{S_{ID}}{I_D^2}\right|_{\Delta N} + \left.\frac{S_{ID}}{I_D^2}\right|_{\Delta\mu} \tag{23}$$

3. Devices and measurements

In order to verify the model, organic p-channel TFTs with a channel width (W) of 100 μm and channel lengths (L) of 40 μm and 20 μm were fabricated on a 125 μm-thick flexible polyethylene naphthalate (PEN) substrate in the inverted staggered (bottom-gate, top-contact) device architecture using polyimide shadow masks [28]. The TFTs consist of 30 nm-thick aluminum gate electrodes, an 8 nm-thick hybrid AlO_x/SAM gate dielectric, a 25 nm-thick vacuum-deposited layer of the small-molecule organic semiconductor DNTT, and 30 nm-thick gold (Au) source and drain contacts [28]. The maximum process temperature was 60 °C.

Protocol for the current–voltage measurements: All transfer characteristics were measured at a drain–source voltage (V_{DS}) of −3.0 V by sweeping the gate–source voltage (V_{GS}) from 0 to −3.0 V with a step size of −50 mV. All measurements were performed in ambient air at room temperature.

Protocol for the LFN measurements: All LFN measurements where performed with the TFTs biased in saturation (V_{DS} = −3.0 V) and with gate–source voltages (V_{GS}) of −1.2 V, −1.5 V, −2.0 V, −2.5 V and −3.0 V. For each applied gate–source voltage, the PSD of the drain-current noise was measured in the frequency range between 1 Hz and 10^5 Hz. All measurements were performed in ambient air at room temperature. Note that small signal measurements were not performed. In the subthreshold regime, a cutoff frequency of approximately 800 Hz and 10 Hz was calculated [29], at the gate–source voltages of −1.5 V and −1.2 V, respectively.

Approximately 15 TFTs of each channel length (20 μm and 40 μm) were measured. The mean-value characteristics were generated from the measured transfer characteristics by calculating the sample-mean $E[I_{DS}]$ of the measured drain current I_{DS} at each applied gate–source voltage. The mean-value transconductance $E[G_m] = \Delta E[I_{DS}]/\Delta V_{GS}$ was approximated from the mean-value transfer characteristics. Each PSD sample of the drain-current noise S_{ID} was multiplied by the corresponding frequency, the average $S_{ID}f$ value was calculated in the frequency range between 10 Hz and 100 Hz, and the mean value of the noise $E[S_{ID}f]$ was calculated by averaging over all TFTs. This procedure was executed for each gate–source voltage at which a noise measurement had been performed. For gate–source voltages in the deep subthreshold regime, the corner frequency value of the noise spectrum is relatively small and thus the white-noise regime is noticeable from lower frequency values [30]. Additionally, in the same biasing regime, the deviation of the noise spectrum from the ideal $1/f$ LFN trend is quite large, leading to AF exponent values smaller than unity [25]. This was taken into account during the calculation of the experimental $S_{ID}f$ values (see Fig. 2).

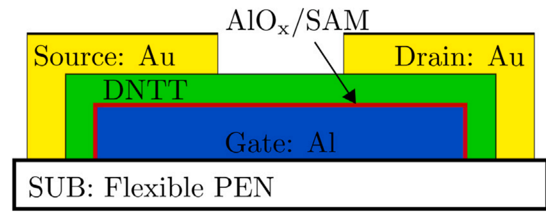

Fig. 2. Schematic cross-section of the organic TFTs fabricated in the inverted staggered (bottom-gate, top-contact) device architecture [9].

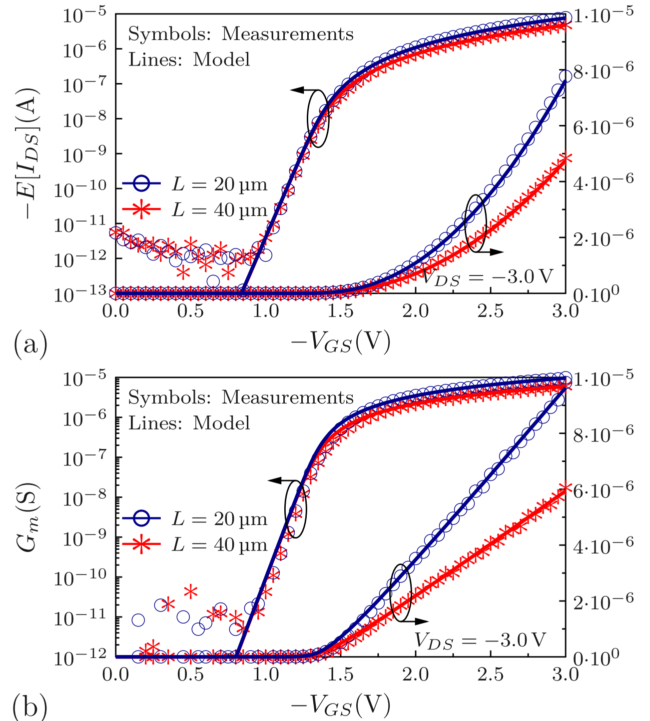

Fig. 3. (a) Mean-value drain current $E[I_{DS}]$ and (b) transconductance g_m plotted versus the gate–source voltage V_{GS} of TFTs with channel lengths of 40 μm and 20 μm. The transfer characteristics were recorded in the saturation regime (V_{DS} = −3.0 V). Symbols: Values calculated from experimental data. Lines: Simulation results.

4. Results and discussion

Fig. 3 shows the mean-value transfer characteristics and the transconductance G_m of TFTs with channel lengths of 40 μm and 20 μm, recorded using the current–voltage-measurement protocol described above. Experimental data and simulation results are shown as symbols and lines, respectively, and both are in good agreement, except for the off-state region (i.e., the range of gate–source voltages between 0 and −0.9 V), which is not covered by the model. For the fabricated TFTs, as previously described in [31], hopping mainly limits the transport. However, in the current work, in order to arrive finally at closed form expressions for the noise figure, a constant effective mobility has

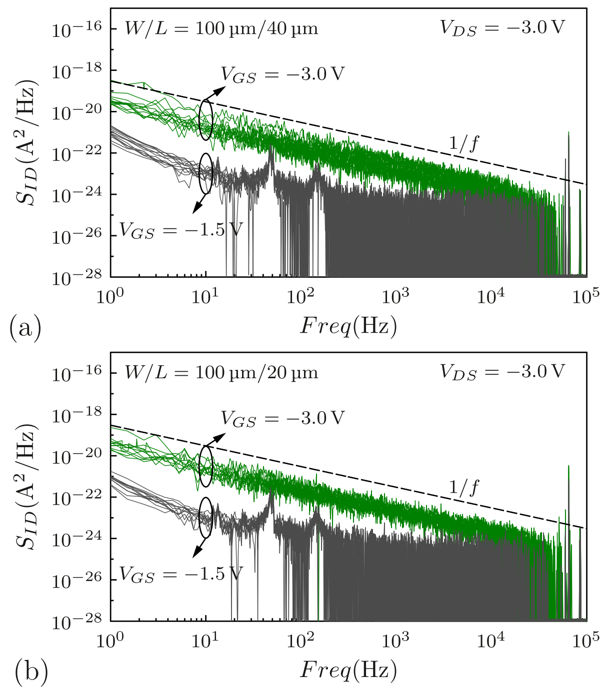

Fig. 4. Flicker-noise spectra of TFTs with channel lengths L of (a) 40 μm and (b) 20 μm, measured at gate–source voltages (V_{GS}) of −1.5 V and −3.0 V and with a drain–source voltage V_{DS} of −3.0 V, i.e., with the TFTs operating in saturation. The dashed line indicates the ideal $1/f$ slope.

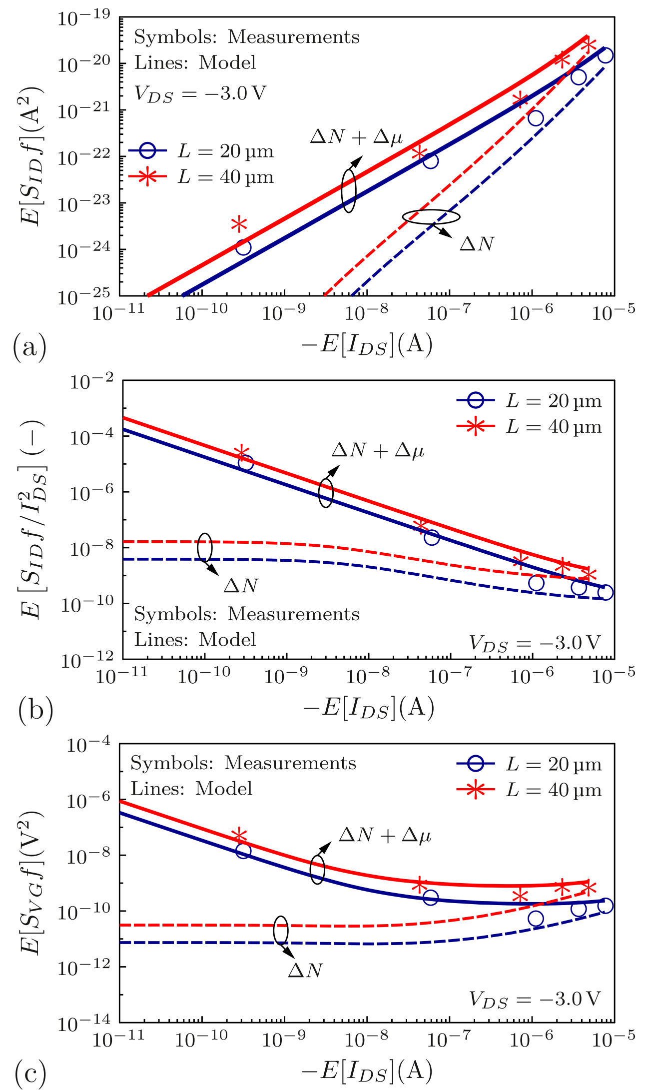

Fig. 5. Power spectral densities (a) S_{ID} and (b) S_{ID}/I_{DS}^2 at a frequency of 1 Hz, measured at a drain–source voltage V_{DS} of −3.0 V and plotted versus the drain current I_{DS}. (c) Input-referred noise $S_{VG}f$ of the same transistors. All measurements were performed with the TFTs biased in saturation (V_{DS} = −3.0 V). Symbols: Values calculated from experimental data. Lines: Simulation results.

been considered, which gives a good approximation according to the transfer characteristics shown in Fig. 3. In Fig. 4, the discrete noise spectra of the TFTs, measured at gate–source voltages (V_{GS}) of −1.5 V (subthreshold regime) and −3.0 V (maximum gate–source voltage), are depicted. In all cases, the measured flicker noise represents typical $1/f^{AF}$ behavior, particularly at lower frequencies between 1 Hz and 100 Hz, a fact which is in agreement with findings presented in [14]. The peaks appeared in the $V_{GS} = -1.5$ V spectra, occur due to the AC power line.

In Fig. 5(a) and (b), the PSDs of the average LFN S_{ID} and S_{ID}/I_{DS}^2 at a frequency of 1 Hz of TFTs with channel lengths of 40 μm and 20 μm are plotted versus the drain current I_{DS}. Both the $S_{ID}f$ and the $S_{ID}f/I_{DS}^2$ PSDs follow a trend that is also typically observed in silicon transistors, namely that the noise is smaller in TFTs that have a smaller active area (product of channel length and channel width) [25]. The $\Delta\mu$ model-component covers the noise behavior at lower drain currents, predicting accurately the observed increase of the noise with decreasing drain current in the subthreshold regime (i.e., for drain currents below about 10^{-7} A), were the $\Delta\mu$ effect is more prominent, similar to silicon transistors [21]. The ΔN model-component is used to predict the measured LFN towards higher drain current. In the subthreshold regime, the distance between localized states is relatively large, which is expected to affect the mobility fluctuation [31], whereas in the above-threshold regime, the hopping distance will be smaller, and thus the effect of the Hooge parameter a_H is expected to be minimal. Overall, the agreement between model ($\Delta N + \Delta\mu$ sum) and experiment is quantitatively satisfactory, both in the below-threshold and the above-threshold regimes of operation.

The noise PSD referred to the gate, $S_{VG} = S_{ID}/G_m^2$, is depicted in Fig. 5(c). As can be seen, the LFN is smaller in the TFTs that have a smaller active area, i.e., a smaller channel length. Again, the model correctly predicts the experimentally measured LFN in both the subthreshold- and the above-threshold regimes.

Table 1 summarizes the values of the parameters N_T, a^* and a_H extracted from the LFN model for each channel length in saturation

Table 1
Extracted parameters of the LFN model.

	N_T ($eV^{-1}cm^{-3}$)	a^* (Vs/m^2)	a_H (−)
$L = 40\,\mu m$	1.3×10^{11}	1465	8.2×10^{-2}
$L = 20\,\mu m$	1.3×10^{10}	1375	7.8×10^{-3}

(V_{DS} = −3.0 V). The trap densities N_T predicted by the model are similar to the values reported previously for organic TFTs [12]. Following a similar approach as in [8], a different set of the model parameters (N_T, a^* and a_H) was extracted for the two different available device geometries. The value of N_T was found to be smaller in the TFTs that have a smaller active area. This finding is consistent with results presented in [8]. The extracted value of the Hooge parameter a_H has also been found to be consistent with the values reported in [32] for several organic-TFT technologies.

5. Conclusions

In conclusion, we have developed a semi-physical bias-dependent charge-based low-frequency noise model for organic thin-film transistors. The proposed model is based on charge carrier-number fluctuation-correlated mobility fluctuation (ΔN) and mobility-fluctuation (Hooge) ($\Delta\mu$) effects, and it can be applied to TFTs fabricated in the inverted staggered device architecture. We have shown that the drain-current noise is smaller in TFTs with a smaller active area. The ΔN effect was found to dominate over the $\Delta\mu$ effect in the above-threshold regime. The observed trend of the drain-current-normalized noise increasing with decreasing drain current in the subthreshold regime can be attributed mainly to the $\Delta\mu$ effect. Regardless of the channel length, the results of the proposed model are in good agreement with the experimentally measured bias-dependent drain-current LFN of organic TFTs, especially in the below and above-threshold regimes.

Declaration of competing interest

The authors declare that they have no known competing financial interests or personal relationships that could have appeared to influence the work reported in this paper.

Data availability

Data will be made available on request.

References

[1] C. Wang, H. Dong, W. Hu, Y. Liu, D. Zhu, Semiconducting π-conjugated systems in field-effect transistors: A material odyssey of organic electronics, Chem. Rev. 112 (4) (2012) 2208–2267.
[2] J.W. Borchert, U. Zschieschang, F. Letzkus, M. Giorgio, R.T. Weitz, M. Caironi, J.N. Burghartz, S. Ludwigs, H. Klauk, Flexible low-voltage high-frequency organic thin-film transistors, Sci. Adv. 6 (21) (2020).
[3] S. Elsaegh, C. Veit, U. Zschieschang, M. Amayreh, F. Letzkus, H. Sailer, M. Jurisch, J.N. Burghartz, U. Würfel, H. Klauk, H. Zappe, Y. Manoli, Low-power organic light sensor array based on active-matrix common-gate transimpedance amplifier on foil for imaging applications, IEEE J. Solid-State Circuits 55 (9) (2020) 2553–2566.
[4] F. Hain, M. Graef, B. Iñíguez, A. Kloes, Charge based, continuous compact model for the channel current in organic thin-film transistors for all regions of operation, Solid-State Electron. 133 (2017) 17–24.
[5] J. Leise, J. Pruefer, G. Darbandy, A. Nikolaou, M. Giorgio, M. Caironi, U. Zschieschang, H. Klauk, A. Kloes, B. Iñiguez, J.W. Borchert, Flexible megahertz organic transistors and the critical role of the device geometry on their dynamic performance, J. Appl. Phys. 130 (12) (2021) 125501.
[6] J. Leise, J. Pruefer, A. Nikolaou, G. Darbandy, H. Klauk, B. Iñiguez, A. Kloes, Macromodel for AC and transient simulations of organic thin-film transistor circuits including nonquasistatic effects, IEEE Trans. Electron Devices 67 (11) (2020) 4672–4676.
[7] J. Pruefer, J. Leise, G. Darbandy, A. Nikolaou, H. Klauk, J.W. Borchert, B. Iñíguez, T. Gneiting, A. Kloes, Compact modeling of short-channel effects in staggered organic thin-film transistors, IEEE Trans. Electron Devices 67 (11) (2020) 5082–5090.
[8] A. Nikolaou, G. Darbandy, J. Leise, J. Pruefer, J.W. Borchert, M. Geiger, H. Klauk, B. Iñiguez, A. Kloes, Charge-based model for the drain-current variability in organic thin-film transistors due to carrier-number and correlated- mobility fluctuation, IEEE Trans. Electron Devices 67 (11) (2020) 4667–4671.
[9] A. Nikolaou, J. Leise, J. Pruefer, U. Zschieschang, H. Klauk, G. Darbandy, B. Iñiguez, A. Kloes, Noise-based simulation technique for circuit-variability analysis, IEEE J. Electron Devices Soc. 9 (2021) 450–455.
[10] L. Ke, S.B. Dolmanan, L. Shen, C. Vijila, S.J. Chua, R.-Q. Png, P.-J. Chia, L.-L. Chua, P.K.-H. Ho, Low frequency noise analysis on organic thin film transistors, J. Appl. Phys. 104 (12) (2008) 124502.
[11] G. Giusi, O. Giordano, G. Scandurra, S. Calvi, G. Fortunato, M. Rapisarda, L. Mariucci, C. Ciofi, Evidence of correlated mobility fluctuations in p-type organic thin-film transistors, IEEE Electron Device Lett. 36 (4) (2015) 390–392.
[12] W.E. Muhea, K. Romanjek, X. Mescot, C.G. Theodorou, M. Charbonneau, F. Mohamed, G. Ghibaudo, B. Iñiguez, 1/f noise analysis in high mobility polymer-based OTFTs with non-fluorinated dielectric, Appl. Phys. Lett. 114 (24) (2019) 243301.
[13] B.R. Conrad, W.G. Cullen, W. Yan, E.D. Williams, Percolative effects on noise in pentacene transistors, Appl. Phys. Lett. 91 (24) (2007) 242110.
[14] M. Deen, O. Marinov, S. Holdcroft, W. Woods, Low-frequency noise in polymer transistors, IEEE Trans. Electron Devices 48 (8) (2001) 1688–1695.
[15] O.D. Jurchescu, B.H. Hamadani, H.D. Xiong, S.K. Park, S. Subramanian, N.M. Zimmerman, J.E. Anthony, T.N. Jackson, D.J. Gundlach, Correlation between microstructure, electronic properties and flicker noise in organic thin film transistors, Appl. Phys. Lett. 92 (13) (2008) 132103.
[16] A. McWhorter, 1/f noise and germanium surface properties, in: R.H. Kingston (Ed.), Sem. Surf. Phys, Univ Penn Press, 1957, pp. 207–228.
[17] F. Hooge, 1/f noise, Physica B+C 83 (1) (1976) 14–23.
[18] A. Kloes, J. Leise, J. Pruefer, A. Nikolaou, G. Darbandy, THM-OTFT compact model.nanoHUB, 2022.
[19] B. Antao, AHD languages-a must for time-critical designs, IEEE Circuits Devices Mag. 12 (4) (1996) 12–17.
[20] J. Pruefer, J. Leise, A. Nikolaou, J.W. Borchert, G. Darbandy, H. Klauk, B. Iñíguez, T. Gneiting, A. Kloes, Compact modeling of nonlinear contact effects in short-channel coplanar and staggered organic thin-film transistors, IEEE Trans. Electron Devices 68 (8) (2021) 3843–3850.
[21] C. Enz, E. Vittoz, Charge-Based MOS Transistor Modeling: The EKV Model for Low-Power and RF IC Design, John Wiley & Sons, Ltd, 2006.
[22] D. Tu, K. Takimiya, U. Zschieschang, H. Klauk, R. Forchheimer, Modeling of drain current mismatch in organic thin-film transistors, J. Disp. Technol. 11 (6) (2015) 559–563.
[23] K.K. Hung, P.K. Ko, C. Hu, Y.C. Cheng, A physics-based MOSFET noise model for circuit simulators, IEEE Trans. Electron Devices 37 (5) (1990) 1323–1333.
[24] H. Agarwal, C. Gupta, P. Kushwaha, C. Yadav, J.P. Duarte, S. Khandelwal, C. Hu, Y.S. Chauhan, Analytical modeling and experimental validation of threshold voltage in BSIM6 MOSFET model, IEEE J. Electron Devices Soc. 3 (3) (2015) 240–243.
[25] A. Nikolaou, N. Mavredakis, M. Bucher, P. Habas, A. Acovic, R. Meyer, Statistical analysis of 1/f noise in enclosed-gate N- and PMOS transistors, in: 2017 International Conference on Noise and Fluctuations, ICNF, 2017, pp. 1–4.
[26] C. Galup-Montoro, M.C. Schneider, H. Klimach, A. Arnaud, A compact model of MOSFET mismatch for circuit design, IEEE J. Solid-State Circuits 40 (8) (2005) 1649–1657.
[27] A. Arnaud, C. Galup-Montoro, A compact model for flicker noise in MOS transistors for analog circuit design, IEEE Trans. Electron Devices 50 (8) (2003) 1815–1818.
[28] M. Geiger, M. Hagel, T. Reindl, J. Weis, R.T. Weitz, H. Solodenko, G. Schmitz, U. Zschieschang, H. Klauk, R. Acharya, Optimizing the plasma oxidation of aluminum gate electrodes for ultrathin gate oxides in organic transistors, Sci. Rep. 11 (1) (2021) 6382.
[29] H. Klauk, U. Zschieschang, M. Halik, Low-voltage organic thin-film transistors with large transconductance, J. Appl. Phys. 102 (7) (2007) 074514.
[30] B. Bahreyni, Chapter 7 - Noise, in: B. Bahreyni (Ed.), Fabrication and Design of Resonant Microdevices, in: Micro and Nano Technologies, William Andrew Publishing, Norwich, NY, 2009, pp. 129–141.
[31] A. Nikolaou, J. Leise, J. Pruefer, U. Zschieschang, H. Klauk, G. Darbandy, B. Iñiguez, A. Kloes, Impact of mechanical bending on the performance of organic thin-film transistors and the characteristic temperature of the density of states, in: 2022 29th International Conference on Mixed Design of Integrated Circuits and System, MIXDES, 2022, pp. 45–50.
[32] T.-C. Fung, G. Baek, J. Kanicki, Low frequency noise in long channel amorphous In–Ga–Zn–O thin film transistors, J. Appl. Phys. 108 (7) (2010) 074518.